Journal of Applied Polymer Science

Synthesis, Antimicrobial Activity, and Release of Tetracycline Hydrochloride Loaded Poly(vinyl alcohol)/Soybean Protein Isolate/Zirconium Dioxide Nanofibrous Membranes

Hualin Wang,[1,3] Yanan Li,[1] Suwei Jiang,[1] Peng Zhang,[1] Sun Min,[1] Shaotong Jiang[2,3]

[1]School of Chemical Technology, Hefei University of Technology, Hefei, Anhui 230009, People's Republic of China
[2]School of Biotechnology and Food Engineering, Hefei University of Technology, Hefei, Anhui 230009, People's Republic of China
[3]Anhui Institute of Agro-Products Intensive Processing Technology, Hefei, Anhui 230009, People's Republic of China
Correspondence to: H. Wang (E-mail: hlwang@hfut.edu.cn)

ABSTRACT: Tetracycline hydrochloride loaded poly(vinyl alcohol)/soybean protein isolate/zirconium (Tet–PVA/SPI/ZrO_2) nanofibrous membranes were fabricated via an electrospinning technique. The average diameter of the PVA/soybean protein isolate (SPI)/ZrO_2 nanofibers used as drug carriers increased with increasing ZrO_2 content, and the nanofibers were uneven and tended to stick together when the ZrO_2 content was above 15 wt %. The Tet–PVA/SPI/ZrO_2 nanofibers were similar in morphology when the loading dosage of the model drug tetracycline hydrochloride was below 6 wt %. The PVA, SPI, and ZrO_2 units were linked by hydrogen bonds in the hybrid networks, and the addition of ZrO_2 improved the thermostability of the polymer matrix. The Tet–PVA/SPI/ZrO_2 nanofibrous membranes exhibited good controlled drug-release properties and antimicrobial activity against *Staphylococcus aureus*. The results of this study suggest that those nanofibrous membranes were suitable for drug delivery and wound dressing. © 2014 Wiley Periodicals, Inc. J. Appl. Polym. Sci. **2014**, *131*, 40903.

KEYWORDS: composites; drug-delivery systems; electrospinning

Received 28 January 2014; accepted 23 April 2014
DOI: 10.1002/app.40903

INTRODUCTION

The electrospinning technique has been endowed with great interest in the fabrication of functional nanofibers because of a broad range of applications, such as drug-delivery devices,[1–3] scaffolds for tissue engineering,[4,5] wound dressing materials,[6,7] artificial organs,[8] and self-cleaning membranes.[9] Some studies have focused on petroleum-derived polymers, including polysulfone,[10] polystyrene,[11] and polyoxymethylene,[12] which are nonbiodegradable under normal environmental conditions. Therefore, natural biopolymers have gained a lot of attention because of their excellent biocompatibility and biodegradability.[13–16]

Soybean protein isolate (SPI) is a biodegradable material extracted from soybeans, which contain more than 90% protein and 18 different amino acids. SPI is a potential substitute for petroleum-derived polymers because of its easy availability and functional properties.[17,18] As it is known, SPI is not convenient to use and process because of brittleness. Moreover, electrospun nanofibers can hardly be produced from pure SPI because it is a globular protein. Attempts have been made to modify SPI to blend it with target polymers.[19–21] Poly(vinyl alcohol) (PVA), a water-soluble polyhydroxy polymer, has been widely investigated for biomedical applications because of its excellent electrospinnability, inherent nontoxicity, biocompatibility, biodegradability, and mechanical properties.[22–27] It is convenient to fabricate SPI/PVA compound nanofibers by an electrospinning technique because both SPI and PVA exhibit hydrogen bonding.[28,29] To improve the properties of SPI/PVA compound nanofibers, we hybridized SiO_2 nanoparticles into the polymer matrix in our early work.[30] It is interesting that ZrO_2 nanoparticles can stimulate nerve tissue and enhance human immunity as a kind of far-infrared material in addition to improving the thermostability of the polymer.[31,32]

Tetracycline hydrochloride (Tet) is a broad-spectrum antibiotic that is effective against Gram-positive and Gram-negative bacteria. Tet was used as a model drug and a representative Gram-positive bacterium. *Staphylococcus aureus* was chosen as test bacterium in this study. The effects of ZrO_2 and the Tet content on the morphology of the nanofibers, and the structure, thermostability, and *in vitro* degradation behavior of the PVA/SPI/ZrO_2 nanofibrous membranes were investigated. Moreover, the Tet release behavior and antimicrobial activity against *S. aureus*

of tetracycline hydrochloride loaded poly(vinyl alcohol)/soybean protein isolate/zirconium (Tet–PVA/SPI/ZrO_2) nanofibrous membranes were emphasized. To the best of our knowledge, no report has been published on the investigation of the fabrication, controlled drug-release behavior, and antimicrobial activity of Tet–PVA/SPI/ZrO_2 nanofibrous membranes via an electrospinning technique for use as a suitable material in drug delivery and wound dressings.

EXPERIMENTAL

Materials

PVA, with a molecular weight of 77,000 ± 2200, and zirconium oxychloride ($ZrOCl_2{\cdot}8H_2O$) was purchased from Sinopharm Chemical Reagent Co., Ltd. (Shanghai, China). SPI was obtained from Nanjin Shiye Co., Ltd. (Shanghai, China). Tet was obtained from Sigma (St. Louis, MO). *S. aureus* was a gift from the School of Biotechnology and Food Engineering, Hefei University of Technology (Anhui, China). All of the other chemical solvents were analytical grade and were available from Sinopharm Chemical Reagent Co., Ltd.

Preparation of the Samples

ZrO_2 Sol. An amount of 6.44 g of $ZrOCl_2{\cdot}8H_2O$ and 2 mL of acetylacetone were added to 30 mL of absolute alcohol and then refluxed at 75°C for 6 h. When the solution was cooled to 25°C, the required H_2O_2 (the molar ratio of H_2O_2 to $ZrOCl_2{\cdot}8H_2O$ used was 3:1) was dripped slowly for about 30 min until the solution was transparent. Subsequently, the solution was aging at room temperature for 10 days to obtain ZrO_2 sol.

Electrospinning Solution. On the basis of our experimental data, a representative 11.7 wt % PVA/SPI mixture (a mixture of PVA and SPI, with a mass ratio of PVA to SPI of 5:1) was chosen to prepare nanofibrous membranes. With the assistance of magnetic stirring, a 12.8 wt % PVA solution was prepared by the dissolution of PVA in deionized water at 100°C for 3 h, and an 8.1 wt % SPI solution was obtained by the dissolution of SPI powder in deionized water (pH 12.0) at 80°C for 30 min. When the PVA solution was added to the SPI solution at 80°C and stirred for 1 h, the needed PVA/SPI mixture was obtained. Finally, the required ZrO_2 sol and Tet were added to the PVA/SPI mixture at 40°C and stirred for 30 min to obtain a homogeneous and transparent electrospinning solutions.

Electrospinning Procedure. The electrospinning device consisted of a syringe, a needle (with a 0.50-mm internal diameter), a copper sheet (8 cm × 8 cm × 0.1 mm), a ground electrode, and a high-voltage power supply (DW-P403-1ACCC, Tianjin Dongwen, China). The supplied voltage was kept at 10 kV, and the tip-to-collector distance was kept at 12 cm. The electrospinning processing was carried out at room temperature. The resulting nanofibrous membranes were dried at 80°C under vacuum conditions for 24 h.

Measurement and Characterization

The morphologies of all of the samples were observed with scanning electron microscopy (SEM; SU8020, Hitachi, Japan), and all of the specimens were sputter-coated with a layer of gold. The SEM images were analyzed by Image Tool software, and a total of 50 counts were used to calculate the average diameter of the nanofibers. X-ray photoelectron spectroscopy (XPS) analysis was performed by Mg Kα radiation with an ESCALAB 250 (Thermo-VG Scientific) X-ray photoelectron spectrometer. Fourier transform infrared (FTIR) spectroscopy was conducted with a Nicolet 6700 spectrometer (Thermo Nicolet) with KBr pellets. Thermostability was evaluated with a TGA 209 thermogravimetric analyzer (Netzsch, Germany). The samples were heated up to 800°C at a constant heating rate of 10°C/min under a nitrogen flow at rate of 50 mL/min.

In Vitro Degradation

The *in vitro* degradation of nanofibrous membranes were carried out in phosphate-buffered saline (PBS; pH 7.2) at 37°C. The square-shaped specimens (10 × 10 mm^2) were immersed in glass vials containing 10 mL of PBS and incubated in a water bath. At predetermined intervals, each sample was rinsed with distilled water to remove the residual PBS and then dried in a vacuum oven maintained at 80°C to a constant weight. The weight loss was calculated according to the following equation:

$$\text{Weight loss}\,(\%) = \frac{m_0 - m_t}{m_0} \times 100\% \quad (1)$$

where m_t is the weight of the specimen at a predetermined time and m_0 is the initial weight of the specimen. The morphological changes of the specimens were observed by SEM during the degradation process.

Drug Release

A series of Tet solutions at concentrations of 6.25, 7.50, 10.00, 12.50, 15.00, 20.00, and 25.00 μg/mL was prepared by the dissolution of Tet into PBS (pH 7.2) at 37°C, respectively. The absorbance at 360 nm was measured for each solution by an ultraviolet spectrophotometer (UV-754PC, China, PBS as a blank). On the basis of the experimental data, the following regression line was determined:

$$Y = 31.25X + 1.25 \left(R^2 = 0.999\right) \quad (2)$$

where X is the absorbance and Y is the Tet concentration (μg/mL).

The release behaviors of the Tet–PVA/SPI/ZrO_2 nanofibrous membranes with different Tet contents were studied in PBS (pH 7.2) at 37°C. The 0.01 g sample was immersed into a 20-mL centrifuge tube containing 10 mL of PBS and put on a shaker platform (100 rpm, 37°C). A volume of 3 mL of PBS was taken from the centrifuge tube, and 3 mL of fresh PBS was added. The absorbances were measured with an ultraviolet spectrophotometer, and the cumulative release percentages of Tet at different times were determined on the basis of eq. (2).

Antibacterial Ability

Assay of the Antibacterial Activity in a Solid Culture Medium. The antimicrobial activity against *S. aureus* in solid culture medium was evaluated with agar disk diffusion. All labware and media had to be sterilized with high-pressure steam before use. We prepared the agar plates were prepared by pouring approximately 15 mL of molten medium into 100 × 15 mm^2 Petri dishes, and then, the plates were allowed to solidify under sterile conditions in a laminar flow. A volume of 1 mL of rejuvenated *S. aureus* suspension was swabbed uniformly

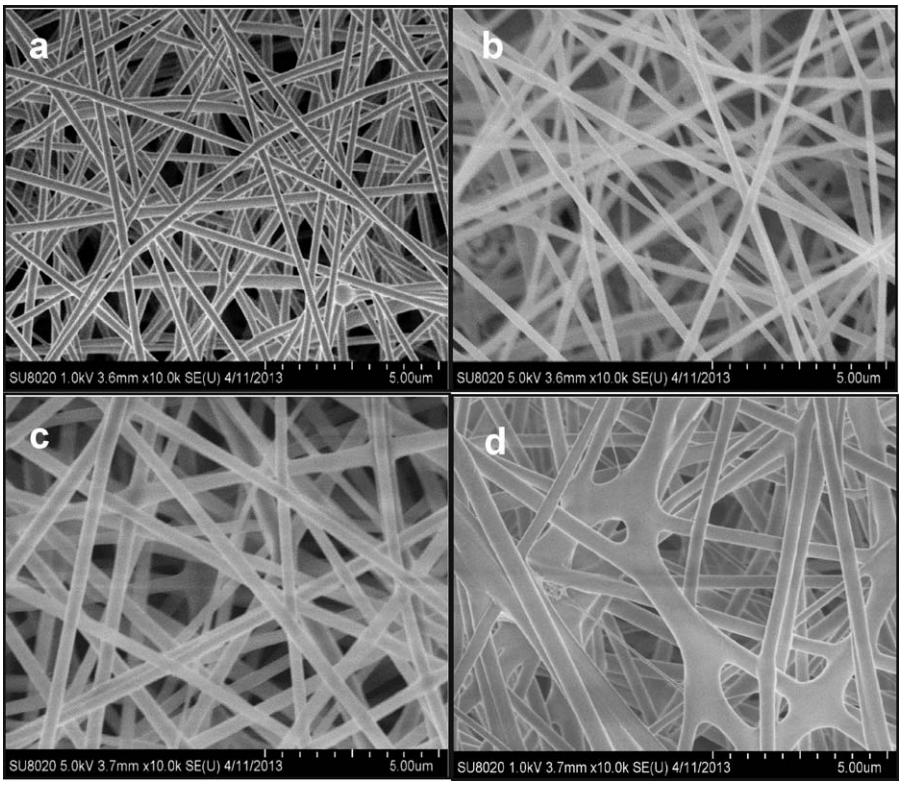

Figure 1. SEM images of PVA/SPI/ZrO_2 nanofibrous membranes with ZrO_2 contents of (a) 0, (b) 5, (c) 10, and (d) 15 wt %.

across the surface of the solid agar culture, and then, a square-shaped copper sheet (0.5 cm × 0.5 cm × 0.1 mm, tailored from the collector of electrospinning setup) was placed on the surface of the solid culture medium, and the side covered with nanofibrous membranes was placed face down onto the agar. The solid culture plates were cultivated in a constant-temperature incubator for 24 h at 37°C. Each sample was repeated three times, and the relative size of the inhibition zone was recorded (copper without nanofibrous membrane was used as a control).

Assay of Antibacterial Activity in a Liquid Culture. The absorbance of the bacterial suspension at 600 nm was directly in accordance with the relative concentration of *S. aureus*. To obtain the regression line, the concentration of *S. aureus* after rejuvenation was set as 1.0. The absorbance was measured at 600 nm for each sample with relative concentrations of *S. aureus* of 0.05, 0.1, 0.2, 0.3, and 0.4 by an ultraviolet spectrophotometer (UV-754PC, China). On the basis of the experimental data, the following regression line was determined:

$$Y = 2.1309X + 0.0229 \left(R^2 = 0.999\right) \quad (3)$$

where X is the relative concentration of *S. aureus* and Y is the absorbance.

A volume of 1 mL of rejuvenated bacterial suspension was transferred into 9 mL of Kings Medium B Agar broth, and then, 30 mg of the Tet–PVA/SPI/ZrO_2 nanofibrous membrane was added to liquid culture medium after sterilization by ultraviolet light for 30 min. The liquid culture media were propagated for 24 h on a shaker platform (160 rpm, 37°C). The absorbances were measured with an ultraviolet spectrophotometer at 600 nm, and the relative concentrations of *S. aureus* were calculated by eq. (3).

RESULTS AND DISCUSSION

Morphologies of the Nanofibrous Membranes

The morphologies of the PVA/SPI/ZrO_2 nanofibrous membranes used as drug carriers with different ZrO_2 contents are shown in Figure 1. As shown, the PVA/SPI nanofibers with average diameter of 235 nm were uniform and smooth on the surface [Figure 1(a)]. The average diameters of the PVA/SPI/ZrO_2 nanofibers with ZrO_2 contents of 5 and 10 wt % were 280 nm [Figure 1(b)] and 430 nm [Figure 1(c)], respectively. Notably, the PVA/SPI/ZrO_2 nanofibers tended to conglutinate when the ZrO_2 content reached 15 wt % [Figure 1(d)]. Because more hydrogen bonds formed among the PVA, SPI, and ZrO_2 units with the addition of ZrO_2 sol. This caused the increase in the viscosity of the electrospinning solution. As a result, the splitting of droplets became more difficult, and the nanofibers became wider during the electrospinning process. When the ZrO_2 content reached 15 wt %, more networks derived from PVA, SPI, and ZrO_2 units prevented the evaporation of the solvent from the gel structure. In this case, the relatively wet nanofibers that reached the collector tended to conglutinate. On the basis of our experimental results, the representative ZrO_2 content at 5 wt % was chosen to prepare the Tet–PVA/SPI/ZrO_2 nanofibrous membranes.

Figure 2 shows the SEM photographs of the Tet-loaded PVA/SPI/ZrO_2 nanofibrous membranes with a ZrO_2 content of 5 wt

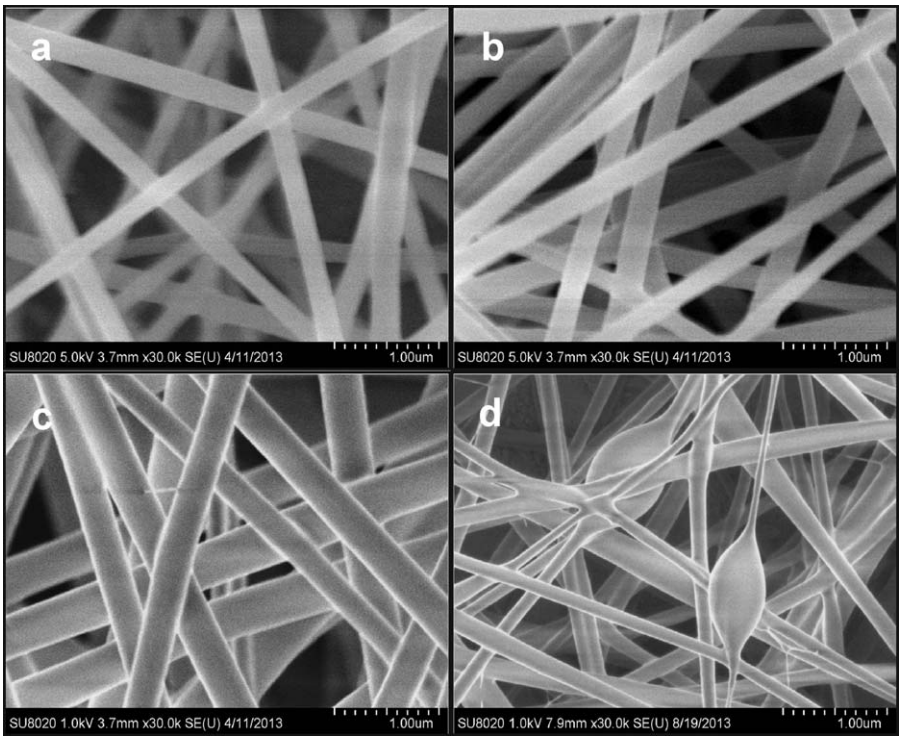

Figure 2. SEM images of PVA/SPI/ZrO_2 nanofibrous membranes (5 wt % ZrO_2) with Tet contents of (a) 2, (b) 4, (c) 6, and (d) 8 wt %.

%. As shown in Figure 2, no Tet particles were observed either on the surface or among the fibers; this revealed that Tet was dispersed uniformly in the PVA/SPI/ZrO_2 matrix in the molecular state. Moreover, the Tet–PVA/SPI/ZrO_2 nanofibers were all smooth and showed an average diameter of about 280 nm when the Tet content was below 6 wt %. This implied that the addition of Tet caused no significant changes in the size and morphology of the nanofibers. Notably, the nanofibers were uneven and interspersed with spindle-shaped beads when the Tet content reached above 8 wt %. The reason might have been that the poor compatibility of Tet in the PVA/SPI/ZrO_2 matrix inhibited the formation of continuous nanofibers during the electrospinning procedures.

Structure, Thermostability, and Degradation of the PVA/SPI/ZrO_2 Nanofibrous Membranes

FTIR Spectral Analysis. Figure 3 presents the FTIR spectra of the PVA nanofibrous membranes, SPI powder, PVA/SPI nanofibrous membranes, zirconia sol, and PVA/SPI/ZrO_2 fibrous membranes. In the FTIR spectrum of PVA [Figure 3(a)], a characteristic peak of the —OH stretching vibrations (strong intermolecular hydrogen bonds) was present at 3378 cm^{-1}, and the —OH bending vibration peak was at 1432 cm^{-1}. The absorption peaks at 2937 and 1090 cm^{-1} were associated with the C—H and C—O stretching vibrations, respectively. In Figure 3(b), the broad band at about 3329 cm^{-1} was due to —NH and —OH stretching vibrations, the peak at 1664 cm^{-1} was due to the C═O stretching vibrations, and the peaks at1547 and 1116 cm^{-1} corresponded to the N—H bending and stretching vibrations; these were in accordance with the data from the reported literature.[33] Compared with Figure 3(a,b), it was revealed in Figure 3(c) that the C═O stretching vibrations moved from 1664 to 1659 cm^{-1}, and the stretching vibrations of —OH shifted to a lower wave number at 3320 cm^{-1}. This indicated that the hydrogen bonds of OH—OH or C═O—HO formed among PVA and SPI. As shown in Figure 3(d), the strong characteristic absorption band at 3416 cm^{-1} was assigned to the stretching vibrations of the —OH groups structured on ZrO_2, and the absorption band at 654 cm^{-1} was attributed to the

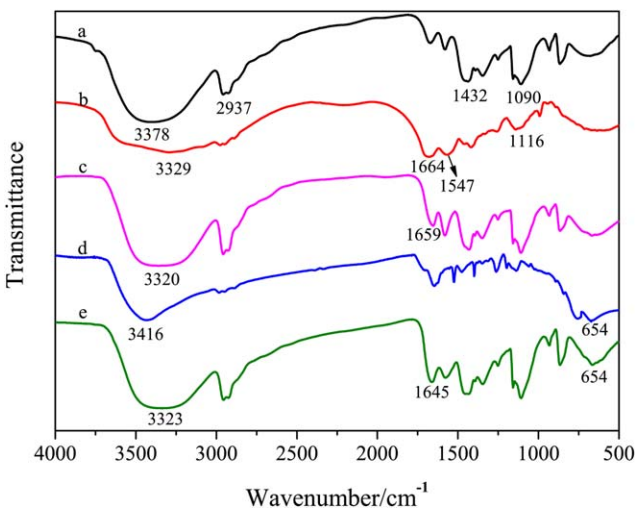

Figure 3. FTIR spectra of samples: (a) PVA fibrous membranes, (b) SPI powder, (c) PVA/SPI fibrous membranes, (d) zirconia sol, and (e) PVA/SPI/ZrO_2 fibrous membranes (5 wt % ZrO_2). [Color figure can be viewed in the online issue, which is available at wileyonlinelibrary.com.]

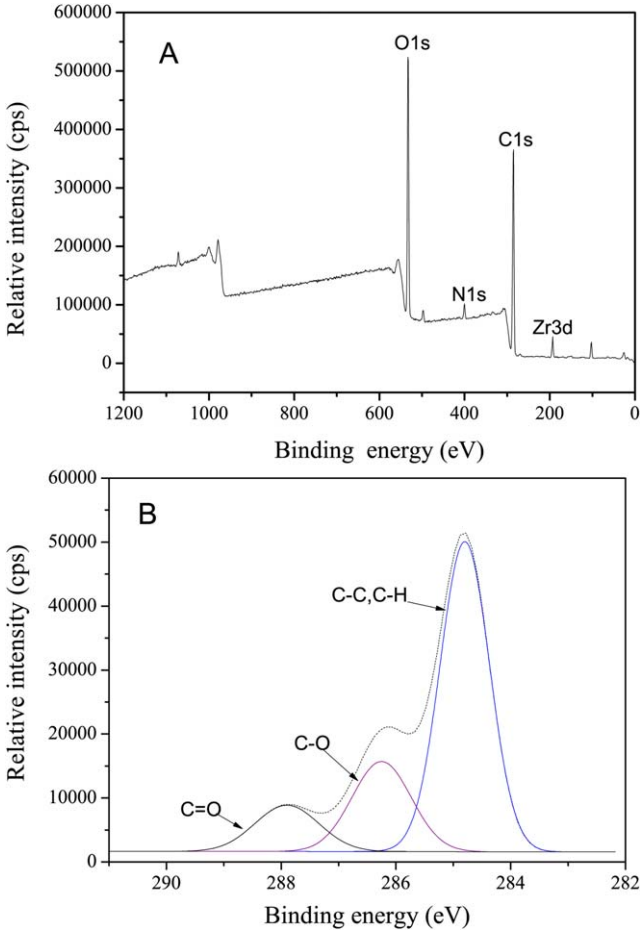

Figure 4. (A) XPS spectra and (B) curve-fitted XPS C1s spectrum of the PVA/SPI/ZrO_2 nanofibrous membranes (5 wt % ZrO_2). [Color figure can be viewed in the online issue, which is available at wileyonlinelibrary.com.]

stretching vibrations of Zr—O—Zr. As shown in Figure 3(e), the characteristic absorption peak at 654 cm^{-1} of Zr—O—Zr was strengthened slightly, and the stretching vibrations of —OH for the PVA/SPI/ZrO_2 nanofibrous membranes shifted to a lower wave number at 3323 cm^{-1} compared to that shown in Figure 3(d), and that of C═O shifted to a lower wave number from 1659 cm^{-1}[Figure 3(b)] to 1645 cm^{-1}. These results suggest that the hydrogen bonds of OH—OH or C═O—HO among the PVA, SPI, and ZrO_2 units were formed.

XPS Analysis. The surface component of the PVA/SPI/ZrO_2 nanofibers with ZrO_2 content at 5 wt % was determined by XPS, and the full-span spectrum is illustrated in Figure 4(A). As shown in Figure 4(A), the peaks for C1s, O1s, N1s, and Zr3d were present at about 285.78, 532.39, 398.97, and 185.69 eV, respectively. When the peak C1s was fitted, three peaks at about 284.8, 286.25, and 287.9 eV were obtained corresponding to C—C, C—O, and C═O, respectively [Figure 4(B)]. These results reveal the existence of C, O, N, and Zr elements and the formation of networks in the PVA/SPI/ZrO_2 nanofibers.

Thermostability Analysis

The thermogravimetric analysis (TGA) curves of the PVA/SPI and PVA/SPI/ZrO_2 nanofibrous membranes are shown in Figure 5. Both TGA curves were similar in shape and could be divided into four main parts. For the PVA/SPI nanofibrous membranes, a weight loss of 7.2% between 50 and 223°C was due to the evaporation of free and coordinated water, the 72.0% weight loss between 223 and 285°C was attributed to the chemical dehydration of the inner molecules and cleavage of C—O and C—C linkages, and the weight loss of 20.6% between 397 and 500°C probably corresponded to the cleavages of S—S, O—N, and O—O linkages.[34] Beyond 500°C, only the char residue remained. In sharp contrast to the PVA/SPI nanofibrous membranes, the PVA/SPI/ZrO_2 nanofibrous membranes exhibited excellent thermostability. As shown in Figure 5, there were weight losses of 10.3% at 50–282°C, 68.2% at 282–336°C, and 16.3% at 398–528°C, and beyond 528°C, more residues remained because of the char and incorporated ZrO_2. These thermogravimetric analyses demonstrated that the initial decomposition temperature of the PVA/SPI/ZrO_2 nanofibrous membranes was 51°C higher than that of the PVA/SPI nanofibrous membranes; this revealed that the thermostability of the PVA/SPI nanofibers prominently increased with the addition of ZrO_2. The reason was that the strong interactions of hydrogen bonds formed among PVA, SPI, and ZrO_2 units delayed the decomposition process. This material could be used in biomedical applications at lower temperatures and functional materials at relatively higher temperatures.

Degradation Behavior. The degradation of the PVA/SPI/ZrO_2 nanofibrous membrane drug carrier played an important role in drug release. Figure 6 shows the SEM photographs of the PVA/SPI/ZrO_2 nanofibrous membranes (5 wt % ZrO_2) degraded in PBS at 37°C. (It was difficult to measure the weight and take an SEM photograph of the PVA/SPI/ZrO_2 nanofibrous membranes when they were degraded into small fragments and dispersed in PBS; therefore, the experimental degradation time used was 10 days.)

At the end of the 1st day, the PVA/SPI/ZrO_2 nanofibers were seriously swollen and partially adhered to one another, but the sketch of the nanofibers was still clear [Figure 6(b)]. At the end

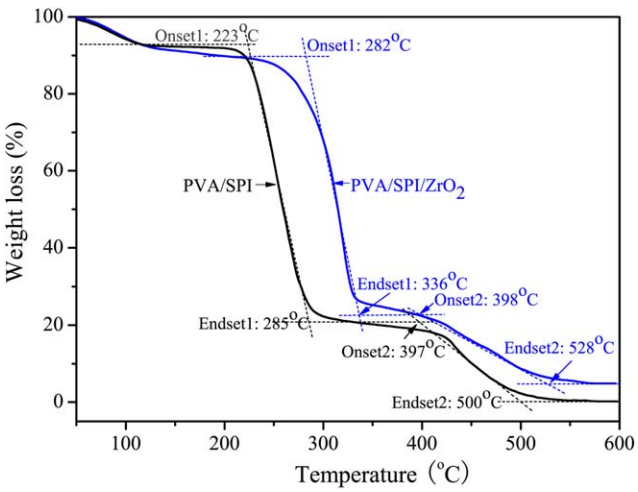

Figure 5. TGA curves of the nanofibrous membranes. [Color figure can be viewed in the online issue, which is available at wileyonlinelibrary.com.]

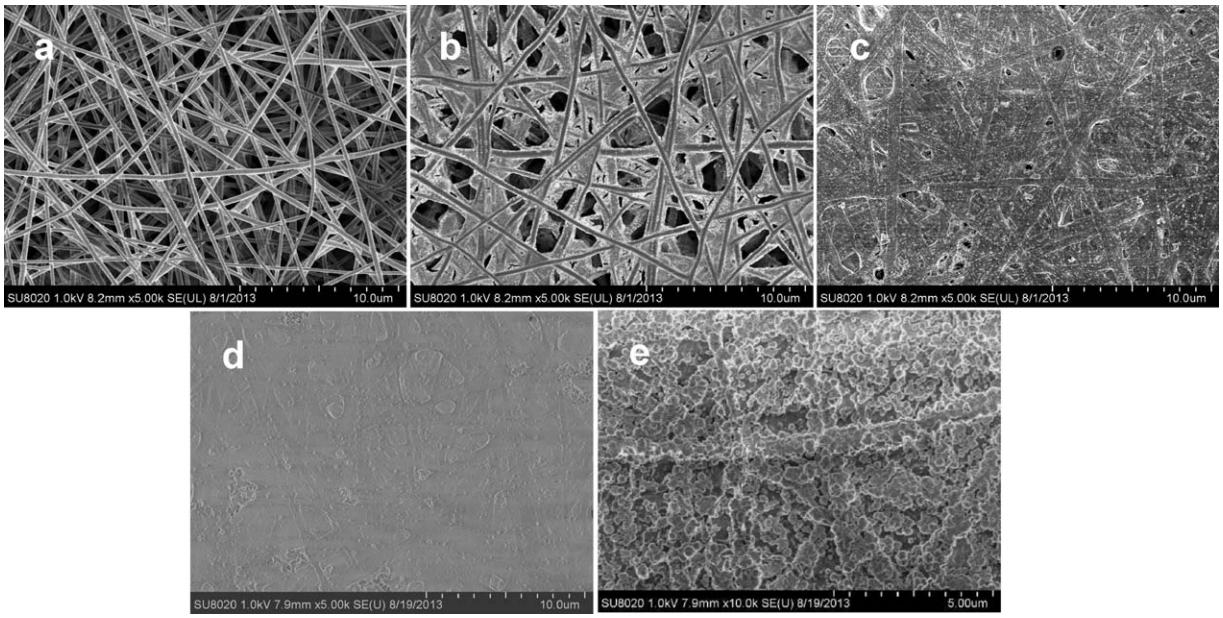

Figure 6. SEM photographs of the PVA/SPI/ZrO_2 fibrous membranes (in PBS at 37°C) at (a) 0, (b) 1, (c) 3, (d) 6, and (e) 10 days.

of 3rd day, the nanofibers were swollen further to form a film, and the sketch of the nanofibers became obscure [Figure 6(c)]. At the end of the 6th day, lots of irregular caves resulting from the dissolution of the degraded polymer were present in the film [Figure 6(d)]. At the end of 10th day, the film had degraded into small fragments [Figure 6(e)]. Figure 7 shows that no obvious weight loss of the PVA/SPI/ZrO_2 nanofibrous membranes and pH change of PBS were found in the first 3 days, and then, the weight loss increased seriously, whereas the pH of PBS decreased slightly. During the first 4 days, water molecules were absorbed on the surface and diffused into the matrix of the nanofibers. Correspondingly, the nanofibers were swollen to form a film, and no obvious weight loss of the nanofibrous membranes or pH change of the PBS were observed. Subsequently, the linkages of the matrix were weakened, and the molecular chains of PVA or SPI began to cleave; moreover, an autoacceleration effect of the degradation phenomenon occurred because carboxyl groups on the cleaved chains derived from SPI could catalyze hydrolytic degradation.[35,36] Accordingly, the weight loss of the nanofibrous membranes increased sharply, and the pH of PBS decreased slightly.

Release Behavior for the Tet–PVA/SPI/ZrO_2 Nanofibrous Membranes

Figure 8 shows the release behavior of the Tet–PVA/SPI/ZrO_2 nanofibrous membranes in PBS. As shown in Figure 8, each nanofibrous membrane showed an initial burst-release phenomenon caused by the dissolution of Tet on the surface of the nanofibers during the first 4 h. The cumulative amount increased gradually from 6.2 to 14.4% when the Tet content increased from 2 to 6 wt % and quickly reached 48.7% when the Tet content rose up to 8 wt %. This phenomenon revealed that Tet could be dispersed into the matrix evenly when the Tet content was below 6 wt %, but the compatibility of Tet in the PVA/SPI/ZrO_2 matrix became worse when the Tet content rose up to 8 wt %. Moreover, the strong interactions among PVA, SPI, and ZrO_2 units may have been partially destroyed by the addition of Tet. Thus, the release percentage of Tet increased with increasing Tet content at each given time. After the initial burst release, the Tet encapsulated in the matrix began to release slowly into the PBS; this was mainly controlled by the diffusion of Tet from the matrix (swelling stage). Finally, the Tet limited by matrix networks released gradually into the PBS; this was mainly controlled by the degradation of the matrix networks among PVA, SPI, and ZrO_2 units (degrading stage). Previous experimental results implied that the PVA/SPI/ZrO_2 nanofibrous membrane drug carrier had good properties of Tet controlled release.

Antimicrobial Activity in the Solid Culture Medium

Zone of inhibition testing is a common method for evaluating the antimicrobial effect of a diffusible agent against microbial

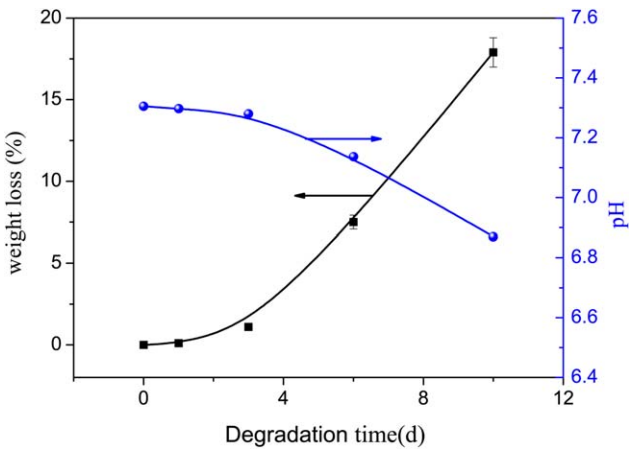

Figure 7. Weight loss and pH changes of the PVA/SPI/ZrO_2 fibrous membranes (in PBS at 37°C). [Color figure can be viewed in the online issue, which is available at wileyonlinelibrary.com.]

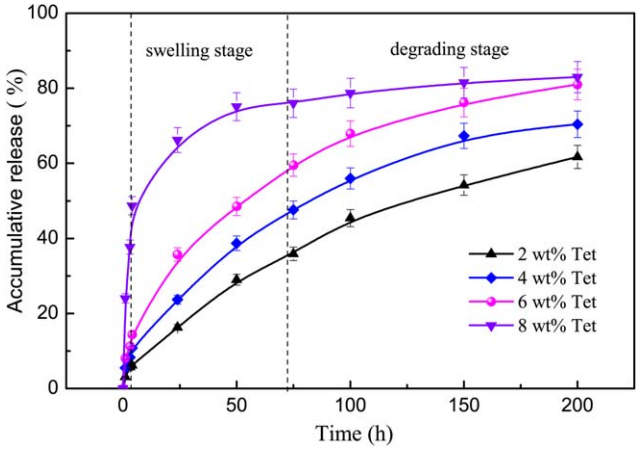

Figure 8. Accumulative amount of Tet released from the Tet–PVA/SPI/ZrO_2 nanofibrous membranes (5 wt % ZrO_2). [Color figure can be viewed in the online issue, which is available at wileyonlinelibrary.com.]

strains of interest.[37] The antimicrobial activity against *S. aureus* of the Tet–PVA/SPI/ZrO_2 nanofibrous membranes were investigated in the solid culture medium, and the results are shown in Figure 9. A clear photograph of the bacterial inhibition zone revealed good antimicrobial activity against *S. aureus* (copper with no nanofibrous membrane as a control was used, and no inhibition zone was found). The diameter of the inhibition zone was enlarged with increasing Tet content when the Tet content was below 6 wt % and then increased in an unobvious manner. The diffusion of Tet in the agar culture medium depended mainly on the Tet content and the agar culture medium resistance; therefore, Tet could spread farther with a higher dosage, but when the diameter of the inhibition zone exceeded a certain value (2.5 cm, 6 wt % Tet), the inhibition zone was enlarged in an unobvious manner because of the diffusion resistance of caused by the agar culture medium.

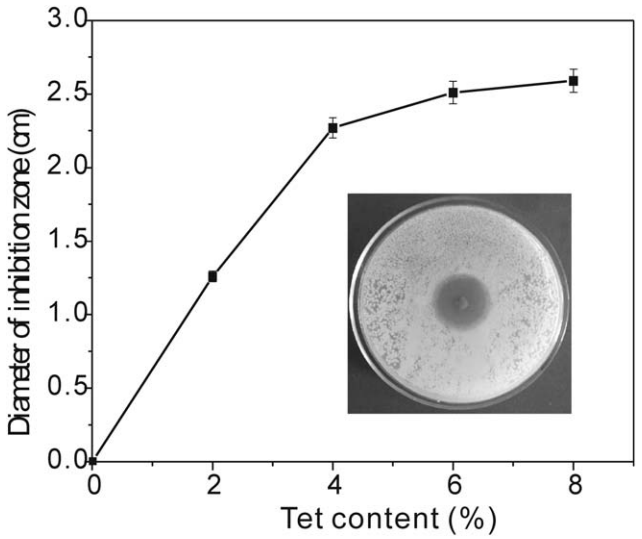

Figure 9. Average diameter of the bacteria inhibition zone of the Tet–PVA/SPI/ZrO_2 nanofibrous membranes (5 wt % ZrO_2) with different Tet contents. The inset is a photograph of the bacteria inhibition zone (6 wt % Tet).

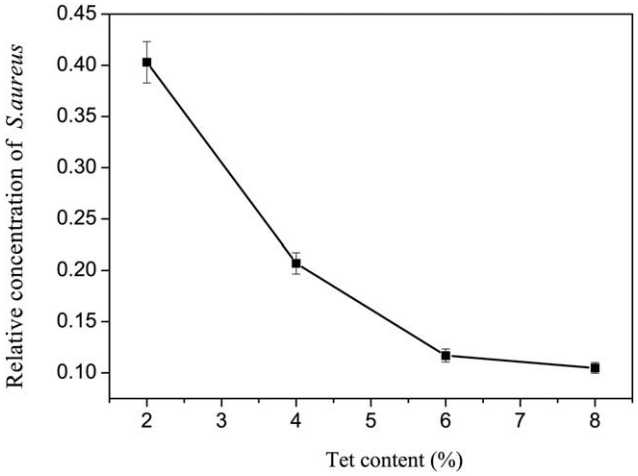

Figure 10. Relative concentrations of *S. aureus* in the samples propagated at 37°C for 24 h.

Antimicrobial Activity in the Liquid Culture Medium

Figure 10 depicts the antimicrobial activity against *S. aureus* of the Tet–PVA/SPI/ZrO_2 nanofibrous membranes with different Tet contents in the liquid culture medium. As shown in Figure 10, the relative concentration of *S. aureus* decreased sharply with increasing Tet content and then decreases unobviously when the Tet content was above 6 wt %. The reason was that the Tet released into the bacterial suspension increased in quantity with increasing Tet content of the Tet–PVA/SPI/ZrO_2 nanofibrous membranes. Thus, the growth of *S. aureus* was effectively inhibited, and the relative concentration of *S. aureus* decreased sharply and correspondingly. Although the Tet content was above 6 wt %, the increase in the Tet content had no obvious effect on the antimicrobial activity against *S. aureus*.

CONCLUSIONS

Tet-loaded PVA/SPI/ZrO_2 nanofibrous membranes were successfully fabricated via an electrospinning technique. The average diameter of the PVA/SPI/ZrO_2 nanofibers used as drug carrier increased with increasing ZrO_2 content, and the nanofibers became uneven and tended to stick together when the ZrO_2 content was above 15 wt %. The loading dosage of the model drug Tet had no obvious effect on the morphology of the Tet–PVA/SPI/ZrO_2 nanofibers when Tet content was below 6 wt %. There existing hydrogen bonds among the PVA, SPI, and ZrO_2 units; this improved thermostability of the composite. The nanofibrous membranes showed an initial burst release during the first 4 h and then releases evenly. The addition of Tet accelerated the degradation of the nanofibrous membranes, and the accumulative release percentage of Tet increased with increasing Tet content. The Tet–PVA/SPI/ZrO_2 nanofibrous membrane exhibited an effective and sustainable inhibition on the growth of *S. aureus*, and the antimicrobial activity increased rapidly with increasing Tet content when the Tet content was below 6 wt %.

ACKNOWLEDGMENTS

Financial support from the National Natural Science Foundation of China (contract grant numbers 31171788 and 31371859) is gratefully acknowledged.

REFERENCES

1. Naveen, N.; Kumar, R.; Balaji, S.; Uma, T. S.; Natrajan, T. S.; Sehgal, P. K. *Adv. Eng. Mater. B* **2010**, *12*, 380.
2. Katti, D. S.; Robinson, K. W.; Ko, F. K.; Laurencin, C. T. *J. Biomed. Mater. Res. Part B: Appl. Biomater.* **2004**, *70*, 286.
3. Nguyen, T. T. T.; Ghosh, C.; Hwang, S.-G.; Chanunpanich, N.; Park, J. S. *Int. J. Pharm.* **2012**, *439*, 296.
4. Kontogiannopoulos, K. N.; Assimopoulou, A. N.; Tsivintzelis, I.; Panayiotou, C.; Papageorgiou, V. P. *Int. J. Pharm.* **2011**, *409*, 216.
5. Kim, M. S.; Park, S. J.; Gu, B. K.; Kim, C. H. *Appl. Surf. Sci.* **2012**, *262*, 28.
6. Charernsriwilaiwat, N.; Opanasopit, P.; Rojanarata, T.; Ngawhirunpat, T. *Int. J. Pharm.* **2012**, *427*, 379.
7. Unnithan, A. R.; Barakat, N. A. M.; Tirupathi Pichiah, P. B.; Gnanasekaran, G.; Nirmala, R.; Cha, Y.-S.; Jung, C.-H.; El-Newehy, M.; Kim, H. Y. *Carbohydr. Polym.* **2012**, *90*, 1786.
8. Shahinpoor, M.; Norris, I. D.; Mattes, B. R.; Kim, K. J.; Sillerud, L. O. *Proc. SPIE Conf.* **2002**, *4695*, 351.
9. Nuraje, N.; Khan, W. S.; Lei, Y.; Ceylan, M.; Asmatulu, R. *J. Mater. Chem. A* **2013**, *1*, 1929.
10. Chang, K. H.; Lin, H. L. *J. Polym. Res.* **2009**, *16*, 611.
11. An, H.; Shin, C.; Chase, G. G. *J. Membr. Sci.* **2006**, *283*, 84.
12. Wang, L.; Peng, P.; Xin, F.; Gao, Y. F.; Yu, J.; Guo, Z. X. *Chem. J. Chin. Univ. Chin.* **2012**, *33*, 620.
13. Kim, C. W.; Kim, D. S.; Kang, S. Y.; Marquez, M.; Joo, Y. L. *Polymer* **2006**, *47*, 5097.
14. Kong, L. Y.; Ziegler, G. R. *Biomacromolecules* **2012**, *13*, 2247.
15. Li, L.; Hsieh, Y. L. *Carbohydr. Res.* **2006**, *341*, 374.
16. Min, B. M.; Lee, G.; Kim, S. H.; Nam, Y. S.; Lee, T. S.; Park, W. H. *Biomaterials* **2004**, *25*, 1289.
17. Cho, S. Y.; Lee, S. Y.; Rhee, C. *LWT—Food Sci. Technol.* **2010**, *43*, 1234.
18. Kokoszka, S.; Debeaufort, F.; Hambleton, A.; Lenart, A.; Voilley, A. *Innov. Food Sci. Emerg. Technol.* **2010**, *11*, 503.
19. Jiang, J.; Xiong, Y. L.; Newman, M. C.; Rentfrow, G. K. *Food Chem.* **2012**, *132*, 1944.
20. Lodha, P.; Netravali, A. N. *Compos. Sci. Technol.* **2005**, *65*, 1211.
21. Lodha, P.; Netravali, A. N. *Ind. Crop. Prod.* **2005**, *21*, 49.
22. Chuang, W. Y.; Young, T. H.; Yao, C. H.; Chiu, W. Y. *Biomaterials* **1999**, *20*, 1479.
23. Gwon, H. J.; Lim, Y. M.; An, S. J.; Youn, M. H.; Han, S. H.; Chang, H. N.; Nho, Y. C. *Korean J. Chem. Eng.* **2009**, *26*, 1686.
24. Li, R. H.; White, M.; Williams, S.; Hazlett, T. *J Biomater. Sci. Polym. Ed.* **1998**, *9*, 239.
25. Paul, W.; Sharma, C. P. *Biomater. Sci. Polym. Ed.* **1997**, *8*, 755.
26. Singh, B.; Sharma, V. *Int. J. Pharm.* **2010**, *389*, 94.
27. Young, T. H.; Yao, N. K.; Chang, R. F.; Chen, L. W. *Biomaterials* **1996**, *17*, 2139.
28. Cho, D.; Nnadi, O.; Netravali, A.; Joo, Y. L. *Macromol. Mater. Eng.* **2010**, *295*, 763.
29. Su, J. F.; Yuan, X. Y.; Huang, Z.; Xia, W. L. *Polym. Degrad. Stab.* **2010**, *95*, 1226.
30. Wang, H. L.; Jiang, Q.; Jiang, S. W.; Jiang, S. T. *Polym. Polym. Compos.* **2012**, *20*, 621.
31. Wey, A. T. C. U.S. Pat. 6,516,229 B1 (**2003**).
32. Wey, A. C. U.S. Pat. 4,590,623 (**2002**).
33. Nanda, P. K.; Rao, K. K.; Kar, R. K.; Nayak, P. L. *J. Therm. Anal. Calorim.* **2007**, *89*, 935.
34. Xu, X.; Jiang, L.; Zhou, Z.; Wu, X.; Wang, Y. *ACS Appl. Mater. Interfaces* **2012**, *4*, 4331.
35. Park, K. E.; Kang, H. K.; Lee, S. J.; Min, B. M.; Park, W. H. *Biomacromolecules* **2006**, *7*, 635.
36. Vey, E.; Roger, C.; Meehan, L.; Booth, J.; Claybourn, M.; Miller, A. F.; Saiani, A. *Polym. Degrad. Stab.* **2008**, *93*, 1869.
37. Bhende, S. M. S.; Spangler, D. M. S. *Infect. Control Hosp. Epidemiol.* **2004**, *25*, 664.